

# A measurement of the broad-band spectrum of XTE J1118+480 with BeppoSAX and its astrophysical implications

F. Frontera<sup>1,2</sup>, A. A. Zdziarski<sup>3</sup>, L. Amati<sup>2</sup>, J. Mikołajewska<sup>3</sup>, T. Belloni<sup>4</sup>, S. Del Sordo<sup>5</sup>, F. Haardt<sup>6</sup>, E. Kuulkers<sup>7</sup>, N. Masetti<sup>2</sup>, M. Orlandini<sup>2</sup>, E. Palazzi<sup>2</sup>, A. N. Parmar<sup>8</sup>, R. A. Remillard<sup>9</sup>, A. Santangelo<sup>5</sup>, L. Stella<sup>10</sup>

## ABSTRACT

We report on results of a target of opportunity observation of the X-ray transient XTE J1118+480 performed on 2000 April 14–15 with the Narrow Field Instruments (0.1–200 keV) of the *BeppoSAX* satellite. The measured spectrum is a power law with a photon index of  $\sim 1.7$  modified by an ultrasoft X-ray excess and a high-energy cutoff above  $\sim 100$  keV. The soft excess is consistent with a blackbody with temperature of  $\sim 40$  eV and a low flux, while the cut-off power law is well fitted by thermal Comptonization in a plasma with an electron temperature of  $\sim 10^2$  keV and an optical depth of order of unity. Consistent with the weakness of the blackbody, Compton reflection is weak. Though the data are consistent with various geometries of the hot and cold phases of the accreting gas, we conclude that a hot accretion disk is the most plausible model. The Eddington ratio implied by recent estimates of the mass and the distance is  $\sim 10^{-3}$ , which may indicate that advection is probably not the dominant cooling mechanism. We finally suggest that the reflecting medium has a low metallicity, consistent with location of the system in the halo.

*Subject headings:* accretion, accretion disks — binaries: general — black hole physics — stars: individual (XTE J1118+480) — X-rays: observations — X-rays: stars

---

<sup>1</sup>Dipartimento di Fisica, Università degli Studi di Ferrara, Via Paradiso 12, I-44100 Ferrara, Italy; frontera@fe.infn.it

<sup>2</sup>Istituto Tecnologie e Studio Radiazioni Extraterrestri, CNR, Via Gobetti 101, I-40129 Bologna, Italy

<sup>3</sup>N. Copernicus Astronomical Center, Bartycka 18, 00-716 Warsaw, Poland; aaz@camk.edu.pl

<sup>4</sup>Osservatorio Astronomico di Brera, Via Bianchi, 46, I-23807 Merate, Italy

<sup>5</sup>Istituto di Fisica Cosmica ed Applicazioni dell'Informatica, CNR, Via U. La Malfa 153, I-90146 Palermo, Italy

<sup>6</sup>Università dell'Insubria, Como, Via Lucini 3, I-22100 Como, Italy

<sup>7</sup>Space Research Organization of Netherlands, Sorbonnelaan 2, 3584 CA Utrecht, NL, and Astronomical Institute, Utrecht University, P.O. Box 80000, 3504 TA Utrecht, NL

<sup>8</sup>Astrophysics Division, Space Science Department of ESA, 2200 AG Noordwijk, The Netherlands

<sup>9</sup>Center for Space Research and Department of Physics, MIT, 77 Mass. Ave., Cambridge, MA 02139, USA

<sup>10</sup>Osservatorio Astronomico di Roma, Via Frascati, 33,

## 1. Introduction

The high Galactic latitude source ( $l = 157.7^\circ$ ,  $b = 62.3^\circ$ ) XTE J1118+480 was discovered in the 2–10 keV energy band with the All-Sky Monitor (ASM) aboard the *Rossi X-Ray Time Explorer (RXTE)* satellite on 2000 March 29 as a weak ( $\sim 40$  mCrab) X-ray source. Retrospective analysis showed that its flux was slowly rising since 2000 March 5 (Remillard et al. 2000) and that another outburst had occurred in 2000 January 2–29, with a similar peak flux on January 6 (Remillard et al. 2000), see Figure 1. The source was also detected in the 20–100 keV band with the *CGRO/BATSE* experiment (Wilson & McCollough 2000): the flux was  $\sim 60$  mCrab on March 26 and  $\sim 110$  mCrab on January 11. The energy spectra derived from the ASM and BATSE data

---

I-00040 Monteporzio Catone, Italy

were described by a power law with photon index of  $\sim 1.8$  and  $\sim 2.1$ , respectively. These power law slopes are typical of black hole binaries (e.g., Cyg X-1) in the hard state.

A radio counterpart of XTE J1118+480 was discovered by Pooley & Waldram (2000) on March 31 with a flux density of 6.2 mJy at a frequency of 15 GHz. Also, the source was detected in the optical and near-infrared bands (Garcia et al. 2000; Chaty et al. 2000; Wren & McKay 2000) with magnitudes of 12.12, 11.75 and 11.06 in the J, H, K bands, respectively, on 2000 April 4.2 (UT), and of 13.11 in the V band on March 28.206. Optical spectroscopy performed on March 31.0 shows H $\alpha$  emission with an FWHM (2200 km s $^{-1}$ ) that is approximately equal to the largest found in black hole X-ray novae during quiescence (Garcia et al. 2000). Observations performed with the *Hubble Space Telescope* (Haswell, Hynes, & King 2000a) on 2000 April 8 show an H $\alpha$  absorption line with full width corresponding to radial velocities likely  $> 10^4$  km s $^{-1}$ , which are suggestive of a massive accretor.

The optical counterpart of XTE J1118+480 is found at R.A. (2000) = 11<sup>h</sup>18<sup>m</sup>10<sup>s</sup>.85 and Decl. (2000) = +48°02'12".9 (Uemura et al. 2000). A star with a 18.8  $R$  magnitude in the USNO A1.0 and A2.0 catalogues is within 2" of that direction, and it has been proposed as the quiescent optical counterpart of the source (Uemura et al. 2000). Its low magnitude is consistent with the LMXB nature of the transient source (Tanaka & Shibazaki 1996). An interesting property of the system in outburst is the very low X-ray-to-optical flux ratio ( $\sim 5$ ) with respect to the typical value of  $\sim 500$  found in LMXBs (van Paradijs & McClintock 1995).

Cook et al. (2000) reported the discovery of a sinusoidal periodic variation of the V-band light curve with a period of 0.1706 days, while a value of  $0.17078 \pm 0.00004$  days has been obtained by Uemura et al. (2000). No evidence of periodicity was found in the soft X-rays (Hynes et al. 2000). The above optical modulations have been interpreted as a superhump (Kuulkers 2001), while the true binary period ( $P = 0.1703$  days) has been determined by McClintock et al. (2000, 2001) and Wagner et al. (2000) through radial velocity studies of the optical counterpart in quiescence. Revnivtsev, Sunyaev, & Borozdin (2000) report

the discovery of a QPO feature at 0.085 Hz in the X-ray light curves from the Proportional Counter Array (PCA) aboard *RXTE*, while the evolution of this QPO for a long time has been investigated by Wood et al. (2000). Besides the QPO, the Power Spectral Density (PSD) shows a strong band-limited noise component (40% fractional rms), also typical of BHCs in their low state. No significant variability was detected at higher frequencies. Similar variations and QPOs were observed in the optical/UV band (Haswell et al. 2000b).

The definite confirmation of the black hole nature of the source has been provided by measurements of the mass function being as large as  $\sim 6M_{\odot}$  (McClintock et al. 2000, 2001a, hereafter M01a; Wagner et al. 2000), rivaled only by that of V404 Cyg. In §2.1 below, we discuss the black hole mass and inclination implied by those and other measurements.

Given the broad energy band of the instrumentation on board *BeppoSAX* (0.1–200 keV) and the high Galactic latitude of the source, XTE J1118+480 could be searched for an ultrasoft component during a hard spectral state with unprecedented sensitivity. As soon as the source became observable with *BeppoSAX*, we started a Target Of Opportunity (TOO) observational program devoted to study the spectral properties of the source. Here we present results of the first observation performed on 2000 April 14–15. In figure 1 we show the epochs of the source observations with *BeppoSAX*.

## 2. Parameters of the System

### 2.1. Masses, inclination and distance

McClintock et al. (2000), M01a and Wagner et al. (2000) have recently detected absorption lines of an M0–M1 V star in their red optical spectra obtained when the object was in a quiescent state. The weighted average of their measurements of the velocity amplitude for the secondary is  $K_2 = 697 \pm 9$  km s $^{-1}$ , which yields the mass function of

$$f(M_2) = \frac{(M_X \sin i)^3}{(M_X + M_2)^2} = 6.0 \pm 0.2 M_{\odot} \quad (1)$$

for  $P = 0.17$  days (where  $i$  is the inclination).

At the same time, Garnavich (2000; see also M01a) found a double sinusoidal variation with a

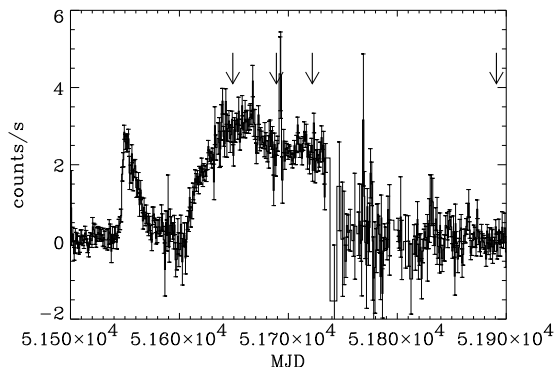


Fig. 1.— One-day-average count rates from XTE J1118+480 detected with the *RXTE*/ASM during the outburst. (From the Internet public archive at [xte.mit.edu/XTE/asmlc/ASM.html](http://xte.mit.edu/XTE/asmlc/ASM.html).) The *BeppoSAX* observations are marked with the arrows. The observation analyzed here is the earliest one.

peak-to-peak amplitude of 0.15 mag in the *I*-band light curve phased to the 0.17-day period. This suggests that the secondary is tidally distorted.

In systems with mass ratios of  $q = M_X/M_2 \gtrsim 1.25$ , the average density of a Roche-lobe-filling secondary is determined solely by the orbital period, which implies simple period–mass–radius–spectral type relations for lower main sequence (MS) secondaries (Frank, King, & Raine 1992). In the case of XTE 1118+480, the orbital period implies a spectral type of M2 and a mass of  $\sim 0.45 M_\odot$  for a MS secondary with near-solar metallicity, whereas a star with lower metallicity would have somewhat earlier spectral type (e.g. Beuermann et al. 1998). An evolved secondary would have a spectral type significantly later than that of a zero-age MS star with the same density (i.e., in a binary with the same orbital period) and a lower mass (e.g. Baraffe & Kolb 2000). If the secondary is a MS star with  $M_2 \simeq 0.45 M_\odot$ , equation (1) yields  $q \gtrsim 15$ , and  $M_X \sin^3 i \gtrsim 6.8 M_\odot$ . The lack of dips or eclipses for a Roche-lobe filling secondary, in particular in the X-ray light curve (Revnivtsev et al. 2000), yields an upper limit for the inclination of  $i < 80^\circ$ , and  $M_X \gtrsim 7.1 M_\odot$ .

The light curve presented in fig. 1 of M01a shows some deviations from a purely ellipsoidal light curve. First, it shows some extra light at

$\sim 0.05P$  after the inferior conjunction of the secondary, which, according to M01a can be explained by a bright spot at the edge of accretion disk. There is also a phase lag of 0.05 relative to the spectroscopic ephemeris, which makes the ellipsoidal nature of the light curve somewhat problematic. On the other hand, M01a found a significant contamination of the visual light by an accretion disk, which likely contaminates also the infrared light. In this case, eclipse effects in an extended disk can possibly shift the phase of the light curve.

Thus, we follow M01a and assume that the light curve is dominated by ellipsoidal effects. The amplitude of the double sinusoid is then positively correlated with  $q$ ,  $i$ , and the Roche-lobe filling factor. Moreover, the two minima of the ellipticity effect are in general unequal, the one corresponding to the superior conjunction of the distorted star being deeper than the other. The magnitude difference between the two minima is a function of  $i$  and the filling factor. In particular, for a Roche-lobe filling star, this difference should be about 0.1 mag for  $i \geq 80^\circ$  decreasing almost linearly to 0 at  $i \sim 40^\circ$ .

The light curve presented by M01a shows the shallower minimum at the inferior conjunction (as expected) of  $\Delta I \sim 0.11$ , and the magnitude difference between the two minima of  $\sim 0.07$ , indicating  $i \geq 60^\circ$ . On the other hand, for  $q \gtrsim 15$  and a Roche-lobe filling star with convective envelope, we estimate the amplitude of the shallower minimum to be  $\Delta I \gtrsim 0.35 \sin^2 i$  mag, which suggests much lower inclination,  $i \simeq 34^\circ$ . This shows that the amplitude of the ellipsoidal variability is reduced due to contamination of the *I*-band flux by some additional contribution from other source(s), e.g. an accretion disk.

M01a found that the secondary contributes 42% (K5V) to 26% (M1V) of the total flux at 5900 Å. To evaluate a contribution of the accretion disk at the *I*-band, we assume that the local disk spectrum corresponds to either  $F_\nu$  or  $F_\lambda$  being constant. Assuming an M1–M2 secondary, we estimate the contribution of the disk as  $\sim 30\%$  and  $\sim 60\%$ , in the first and second case, respectively.

Then, the following equations can be used to determine  $q$ ,  $i$ , and the binary separation,  $a$ . Ke-

pler’s third law reads,

$$M_X + M_2 = 0.01343 \frac{(a/R_\odot)^3}{(P/1 \text{ day})^2} M_\odot. \quad (2)$$

The secondary’s radial velocity amplitude,  $K_2 = 697 \text{ km/s}$ , corresponds to

$$a \sin i = 2.34 \frac{1+q}{q} R_\odot. \quad (3)$$

The full (peak-to-peak) amplitude produced by the tidal distortion is

$$\Delta I = 4.3q \left( \frac{R_t}{a} \right)^3 \sin^2 i \text{ mag}, \quad (4)$$

where  $R_t$  corresponds to the “transverse radius” of the secondary, which is about 96% of the mean radius,  $R_2$ , of its Roche lobe. The numerical coefficient in equation (4) was evaluated from synthetic  $I$ -band light curves generated with the Wilson-Devinney code (Wilson 1990) using a gravity-darkening exponent of 0.32, a linear limb-darkening coefficient of 0.6, and using the shallower minimum in the synthetic light curve. Assuming a MS secondary with  $M_2 \simeq 0.45M_\odot$  and  $R_2 \simeq 0.45R_\odot$ , we obtain  $a = 3.5R_\odot$ ,  $q = 44$ ,  $i = 43^\circ$ ,  $M_X = 20M_\odot$ , and  $a = 2.8R_\odot$ ,  $q = 22$ ,  $i = 61^\circ$ ,  $M_X = 10M_\odot$  in the cases with constant  $F_\nu$  and  $F_\lambda$ , respectively. The first solution produces equal minima, which is not observed, whereas the second one results in a too shallow second minimum.

On the other hand, the presence of extra light near the first minimum will reduce its depth, whereas the second minimum may be not affected. Using only the depth of the second minimum, we get  $a = 3.13R_\odot$ ,  $q = 31$ ,  $i = 50^\circ$ ,  $M_X = 14M_\odot$  in the first case, and a solution similar to that of M01a,  $a = 2.53R_\odot$ ,  $q = 16$ ,  $i = 80^\circ$ ,  $M_X = 7.1M_\odot$ , in the second case. Note that the first solution still produces equal minima in the light curve.

We note that the determinations of the binary parameters by M01a and above supersede analogous constraints of Dubus et al. (2001), obtained before the recent measurements of  $K_2$ . Those authors used instead the peak-to-peak separation of very broad double-peaked H $\alpha$  Balmer and HeII 4686 Å emission lines, measured by them as  $\Delta v \approx 1270, 1470 \text{ km/s}$ , respectively. They then assumed that  $\Delta v$  represents the projected Keplerian velocity of the outer disk, and used a theoretical value

of its radius,  $R_d$ . For a Keplerian disk with a power-law emissivity, the relation,

$$1 + q^{-1} = \left( \frac{\Delta v}{2K_2} \right)^2 \frac{R_d}{a}, \quad (5)$$

is satisfied (e.g. Smak 1981). However, with the measured  $K_2$ ,  $1 + q^{-1} \approx 0.8R_d/a, 1.1R_d/a$  for the Balmer and HeII lines, respectively. This implies  $R_d \sim a$  for any value of  $q$ , which then appears to invalidate their adopted assumption of a Keplerian outer disk.

Summarizing, the present most likely range of the mass and inclination is

$$60^\circ \lesssim i \lesssim 80^\circ, \quad 10 \lesssim M_X/M_\odot \lesssim 7. \quad (6)$$

The lower and upper limit on  $i$  follow from the unequal light-curve minima and the lack of eclipses, respectively.

The presence of the M1–2 V star with  $V \simeq 20.4$  (M01a) implies the distance of

$$d \simeq (1.3–1.9) \text{ kpc}, \quad (7)$$

where the error also takes into account the uncertainty in the interstellar absorption (see below). We also assumed  $M_V \simeq 8.96–9.9$  for such a MS star with near-solar metallicity (Baraffe & Chabrier 1996). Note that  $d$  will become lower for lower metallicity (Beuermann et al. 1998).

## 2.2. The hydrogen column density

An accurate determination of the hydrogen column density,  $N_H$ , is of key importance for determining the correct spectral model for the source emission. Given the high Galactic latitude of the source, the total Galactic column density along the source direction is likely to be close to  $N_H$ , as well as it represents an upper limit to it. The Galactic column density of HI has been measured in radio in 5 directions within  $1^\circ$  of the direction of the optical counterpart, yielding the range of  $N_{H,G} = (1.28–1.44) \times 10^{20} \text{ cm}^{-2}$  (Dickey & Lockman 1990, as implemented in the FTOOLS software package). The measurement in the direction closest ( $0.29^\circ$ ) to that of XTE J1118+480 gives  $1.28 \times 10^{20} \text{ cm}^{-2}$ , and the average weighted by the angular distance from the source direction is  $1.34 \times 10^{20} \text{ cm}^{-2}$ . We note that, at these low values of  $N_H$ , absorption is effective only at

soft X-rays, at which HI is indeed the main absorbing species. A lower Galactic column density ( $0.75 \times 10^{20} \text{ cm}^{-2}$ ) along the line of sight is derived following Schlegel, Finkbeiner & Davis (1998), who obtained full-sky dust maps on the basis of the *COBE* and *IRAS* satellite data. The uncertainty in their reddening maps is estimated to be about 16%. Taking into account that the  $N_{\text{H}}$  value along the line of sight, obtained by interpolation from these and HI maps, can differ from the real value by a factor  $\sim 2$  (Faison et al. 1998), we can state that the above  $N_{\text{H}}$  estimates are consistent each other.

Then, Dubus et al. (2001) have found 3 weak absorption features (CaII 3933 Å doublet and 3968 Å), interpreted as coming from 3 interstellar clouds in the line of sight moving at different velocities. From best-fitting, they obtain the total  $N_{\text{CaII}} \simeq 1.4 \times 10^{12} \text{ cm}^{-2}$  (without giving its uncertainty). They then convert this value to  $N_{\text{H}}$  using an average range of  $\langle \log(N_{\text{H}}/N_{\text{CaII}}) \rangle \approx 8.1$ – $8.5$  obtained for high-altitude lines of sight (Sembach & Danks 1994). This yields  $N_{\text{H}}$  in the range of  $(1.76$ – $4.4) \times 10^{20} \text{ cm}^{-2}$ . We note, however, that it is sufficient that the actual  $N_{\text{H}}/N_{\text{CaII}}$  ratio in the direction of XTE J1118+480 is just  $\sim 25\%$  less than the lower limit of the above *average* ratio range to achieve the consistency of  $N_{\text{H}}$  from radio mapping of HI with that from CaII. In fact, the H and K lines of CaII correlate poorly with  $N_{\text{H}}$  in general and are thus considered not suitable for the purpose of accurate determination of  $N_{\text{H}}$  (Dickey & Lockman 1990 and references therein).

On the other hand, Hynes et al. (2000) obtained  $N_{\text{H}}$  in the range of  $(0.35$ – $1.15) \times 10^{20} \text{ cm}^{-2}$  by fitting their 0.1–0.2 keV *EUVE* spectrum by a power law with a range of indices. We note that such narrow-band fits appear to be easily subject to systematic errors due to the possibility that the actual spectrum is not a power law. Our *BeppoSAX* data include this range, and we have found  $N_{\text{H}} \sim (0.7$ – $1.5) \times 10^{20} \text{ cm}^{-2}$  by fitting a range of models. Power-law models gave lower values of  $N_{\text{H}}$ , consistent with Hynes et al. (2000), but models with blackbody and Comptonized blackbody spectra gave higher  $N_{\text{H}}$ , consistent with the measurements of Dickey & Lockman (1990). Given the results above, we consider the most likely range of  $N_{\text{H}}$  to be  $\sim 1$ – $1.5 \times 10^{20} \text{ cm}^{-2}$ .

### 3. The Observation and Spectral Data

The observation was performed with the *BeppoSAX* Narrow Field Instruments (NFIs). The *RXTE*/ASM light curve of XTE J1118+480 in the 2–10 keV energy band with the mark of the *BeppoSAX* observations is shown in Figure 1. The NFIs embody a Low Energy Concentrator Spectrometer (LECS, 0.1–10 keV, Parmar et al. 1997), 2 Medium Energy Concentrators Spectrometers (MECS, 1.3–10 keV, Boella et al. 1997), a High Pressure Gas Scintillator Proportional Counter (HPGSPC, 3–100 keV, Manzo et al. 1997), and a Phoswich Detection System (PDS, 15–300 keV, Frontera et al. 1997). The LECS and MECS have imaging capabilities, while the HPGSPC and PDS are collimated detectors with a Field of View (FOV) of  $1^\circ$  and  $1.3^\circ$ , respectively. The PDS instrument makes use of rocking collimators for background monitoring.

We observed the source from 2000 April 14.489 UT to 15.528 UT. The source exposure times were 21197 s, 29758 s, 42138 s, and 20146 s for the LECS, MECS, HPGSPC and PDS, respectively. Useful data were selected from time intervals that met the following criteria: the satellite outside the South Atlantic Geomagnetic Anomaly, the elevation angle above the Earth limb by  $\geq 5^\circ$ , dark Earth (for LECS), stabilized high voltage supplies.

The source was detected with all the NFIs, from  $\sim 0.1$  to 200 keV. The LECS and MECS source spectra were extracted from a region with a radius of  $8'$  around the centroid of the source image. As background spectra we used standard files obtained from the observation of blank fields. The 2 MECS spectra were equalized and co-added. We used background spectra accumulated from dark Earth data for the HPGSPC (note that the instrument's collimator was kept on the source for the entire observation). The background level of the PDS was estimated by swapping its collimators off source every 96 s. The energy bands used for spectral fitting were limited to those where the response functions were best known, i.e. 0.12–4 keV, 1.7–10 keV, 7–29 keV, and 15–200 keV, for the LECS, MECS, HPGSPC and PDS, respectively. The count rate spectra were analyzed using the XSPEC software package (Arnaud 1996). A systematic error of 1% was added in quadrature to

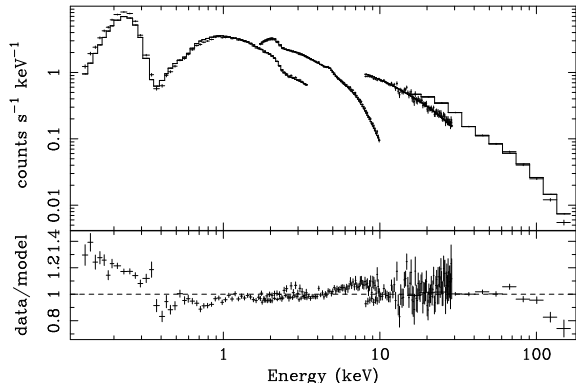


Fig. 2.— *Top panel:* The 0.1–200 keV count rate spectrum of XTE J1118+480. *Bottom panel:* Ratio between the count rate spectrum and the power-law model absorbed by the Galactic  $N_{\text{H}}$ . A soft X-ray excess and a high-energy cutoff are clearly highly significant.

the statistical uncertainties of the spectral data, on the basis of the calibration results obtained with the Crab Nebula, that was observed 4 days before our observation (10 April 2000). We allowed for free normalization of the instruments in multi-instrument fits with respect to MECS. For clarity of display, the unfolded spectra from multi-instrument fits were renormalized to the MECS level.

The results below have been obtained with the spectra averaged over the entire observation. We have also performed a spectral analysis on different time intervals, but have not found any statistically significant variation of the best-fit parameters with time.

The quoted errors for the spectral parameters correspond to 90% confidence for one parameter ( $\Delta\chi^2 = 2.71$ ). The elemental abundances are with respect to those of Anders & Ebihara (1982), and the opacities are from Morrison & McCammon (1983). In calculations of Compton reflection and in Comptonization models in planar geometry, we assume an inclination of  $i = 70^\circ$  (see §2.1).

#### 4. Results

The 0.1–200 keV count rate spectrum obtained with the NFIs (see Figure 2, top panel) was fit with different models. A simple power-law model (PL) with  $N_{\text{H}} = 1.28 \times 10^{20} \text{ cm}^{-2}$  (see §2.2) gives an

unacceptable fit with the photon index,  $\Gamma = 1.81$ , and a very large  $\chi^2/\nu = 1143/231$ , caused mostly by strong systematic residuals at the lowest and highest energies, corresponding to a soft X-ray excess at  $\lesssim 0.5 \text{ keV}$  and a high-energy cutoff at  $\gtrsim 100 \text{ keV}$ , respectively, as shown in the bottom panel of Figure 2. The high energy cutoff is also apparent from figure 3, where we show the ratio of the XTE J1118+480 spectrum measured by the PDS with the corresponding one of the Crab Nebula, which was observed for cross-calibration purposes 4 days before our observation. Replacing the power law with an e-folded power law (CUTOFFPL) and maintaining the  $N_{\text{H}}$  value fixed to  $1.28 \times 10^{20} \text{ cm}^{-2}$  only marginally improve the fit ( $\chi^2/\nu = 1136/230$ ): the systematic residuals at low and high energies are still there (see Figure 2), and the best fit cut-off energy is very high and unconstrained. Only allowing a free  $N_{\text{H}}$  the fit does improve significantly, to  $\chi^2/\nu = 319/229$ , but only for an  $N_{\text{H}} = 0.66^{+0.03}_{-0.03} \times 10^{20} \text{ cm}^{-2}$ , about a half of  $N_{\text{H,G}}$ , even if consistent with the  $N_{\text{H}}$  based on the dust IR maps (§2.2). However still there remain strong systematic residuals at the lowest and highest energies, as confirmed by the still unacceptable  $\chi^2$ . Thus we added to the previous model a blackbody spectrum (BB). With this additional component the fit quality significantly increased ( $\chi^2/\nu = 272/227$ ), with a chance probability that the lower  $\chi^2$  is due to chance of  $1.4 \times 10^{-8}$ . Even if the CUTOFFPL model component is not the best description of the high energy cut-off (see below), it represents a great improvement with respect to a PL component, that gives a much worse and unacceptable quality of the fit ( $\chi^2/\nu = 388/228$ ). This result confirms the statistical significance of the high energy cut-off in our data. The best fit model with BB plus CUTOFFPL provides an  $N_{\text{H}}$  close to  $N_{\text{H,G}}$  with a rather low temperature ( $kT_{\text{bb}} \simeq 50 \text{ eV}$ ) of the BB spectrum, see Table 1. Figure 4 shows the best fit curve along with the residuals of the data to the model.

Still, even the last fit shows strong systematic residuals at the highest energies, as an e-folded power law does not reproduce the actual shape of the high-energy cutoff in the data. Therefore, we have tested models with the main continuum component given by Comptonization, a common physical process in compact sources (see Zdziarski 2000 for a review). We first consider the thermal-

TABLE 1  
FIT RESULTS OF THE 0.1–200 KEV SPECTRUM OF XTE J1118+480

Parameter	BB+CUTOFFPL	BB+COMPTT sph	BB+COMPPS sph, $Z/Z_{sun} = 1$	BB+COMPPS sl, $Z/Z_{sun} = 1$	BB+COMPPS sph, $Z/Z_{sun}$ free	BB+COMPPS sl, $Z/Z_{sun}$ free	BB+COMPPS sph, $kT_{seed} = 10$ eV	BB+COMPPS sl, $kT_{seed} = 10$ eV
$N_H$ [ $10^{20}$ cm $^{-2}$ ]	$1.00^{+0.17}_{-0.12}$	$0.85^{+0.22}_{-0.25}$	$1.45^{+0.27}_{-0.28}$	$1.43^{+0.22}_{-0.16}$	$1.49^{+0.17}_{-0.18}$	$1.50^{+0.18}_{-0.17}$	$1.46^{+0.33}_{-0.36}$	$1.73^{+0}_{-0}$
$kT_{bb}$ [eV]	$52^{+10}_{-10}$	$44^{+10}_{-4}$	$36^{+2}_{-3}$	$36^{+5}_{-4}$	[36]	[36]	$35^{+6}_{-4}$	$32^{+4}_{-2}$
$L_{bb}$ [ $10^{34}$ erg/s] <sup>a</sup>	$0.8^{+0.6}_{-0.3}$	$0.8^{+0.6}_{-0.5}$	$2.2^{+2.6}_{-1.5}$	$2.5^{+2.6}_{-1.8}$	$2.1^{+0.9}_{-0.7}$	$2.6^{+1.0}_{-0.6}$	$3.1^{+4.8}_{-2.8}$	$5.8^{+5}_{-3}$
$R_{bb}/R_g$ <sup>b</sup>	$9^{+5}_{-4}$	$13^{+8}_{-5}$	$32^{+19}_{-12}$	$35^{+20}_{-15}$	$32^{+7}_{-5}$	$35^{+7}_{-4}$	$41^{+34}_{-21}$	$67^{+22}_{-22}$
$kT_{seed}$ [eV]	-	$= kT_{bb}$	$= kT_{bb}$	$= kT_{bb}$	$= kT_{bb}$	$= kT_{bb}$	[10]	[10]
$\Gamma$	$1.722^{+0.003}_{-0.005}$	-	-	-	-	-	-	-
$E_f$ or $kT$ [keV]	$389^{+64}_{-45}$	$239^{+59}_{-60}$	$58^{+12}_{-6}$	$46^{+5}_{-3}$	$78^{+25}_{-17}$	$63^{+20}_{-11}$	$86^{+35}_{-21}$	$68^{+17}_{-12}$
$\tau$	-	$0.53^{+0.20}_{-0.11}$	$2.00^{+0.42}_{-0.21}$	$0.90^{+0.10}_{-0.06}$	$1.49^{+0.48}_{-0.33}$	$0.64^{+0.20}_{-0.11}$	$1.35^{+0.55}_{-0.33}$	$0.59^{+0}_{-0}$
$\Omega/2\pi$	-	-	$\leq 0.17$ ( $2\sigma$ )	$\leq 0.15$ ( $2\sigma$ )	$0.11^{+0.07}_{-0.06}$	$0.16^{+0.11}_{-0.06}$	$0.14^{+0.09}_{-0.07}$	$0.18^{+0}_{-0}$
$Z/Z_\odot$	-	-	[1]	[1]	$0.14^{+0.12}_{-0.09}$	$0.10^{+0.11}_{-0.06}$	$0.17^{+0.17}_{-0.10}$	$0.10^{+0}_{-0}$
$I_{line}$ [ $10^{-4}$ cm $^{-2}$ s $^{-1}$ ]	-	-	$\leq 2.4$ ( $2\sigma$ )	$\leq 2.4$ ( $2\sigma$ )	$\leq 2.4$ ( $2\sigma$ )	$\leq 2.4$ ( $2\sigma$ )	$\leq 2.5$ ( $2\sigma$ )	$\leq 2.4$ ( $2\sigma$ )
$\chi^2/\nu$	272/227	273/227	255/225	263/225	247/225	246/225	244/224	244/224

NOTE.—sph = sphere; sl = slab

<sup>a</sup>Scaled to  $d = 1$  kpc.

<sup>b</sup> $R_{bb}$  scaled at  $d = 1.5$  kpc and  $R_g \equiv GM_X/c^2$  scaled at  $10M_\odot$ .

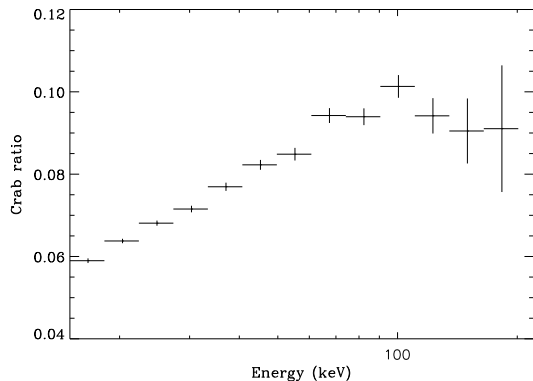


Fig. 3.— Ratio between the count spectrum of XTE J1118+480 and that of Crab observed with *BeppoSAX* 4 days before our TOO measurement. The break in the ratio at  $\sim 100$  keV is apparent.

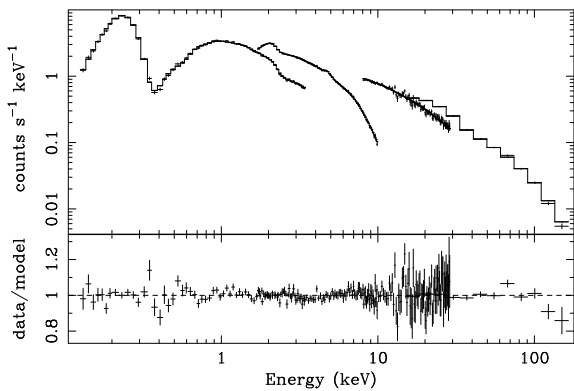


Fig. 4.— *Top panel:* The 0.1–200 keV count rate spectrum of XTE J1118+480, superposed with the best fit model consisting of an absorbed BB plus CUTOFFPL (see text). *Bottom panel:* Ratio between the count spectrum and the model.

Compton model (COMPTT) of Titarchuk (1994), in which a Wien spectrum undergoes scattering in either spherical or slab geometry, and relativistic effects are taken into account. We have found that fits with very similar electron temperature,  $kT$ , and  $\chi^2$  are obtained for either geometry. Similarly to the case of an e-folded power law, the absorbed COMPTT model yields an implausibly low  $N_H$  ( $0.51_{-0.18}^{+0.08} \times 10^{20} \text{ cm}^{-2}$ ) with a  $\chi^2/\nu = 283/228$ , similar to that found with the last model (BB plus CUTOFFPL). Adding an absorbed BB component, with  $T_{\text{bb}}$  equal to the tem-

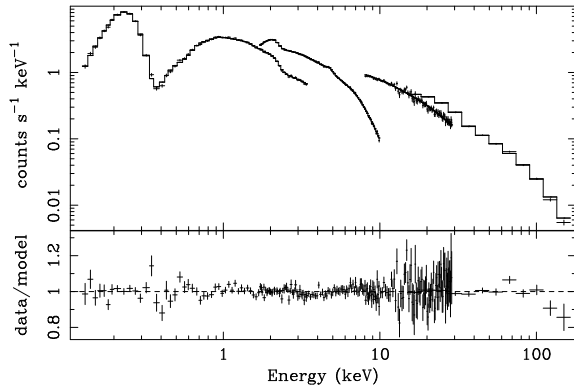


Fig. 5.— *Top panel:* The 0.1–200 keV count rate spectrum of XTE J1118+480, superposed with the best fit model consisting of an absorbed BB plus COMPTT in the spherical geometry (see text). *Bottom panel:* Ratio between the count spectrum and the model.

perature of the seed photons, the best fit  $N_H$  is closer to  $N_{H,G}$ , even though the fit quality does not improve ( $\chi^2/\nu = 279/227$  or  $280/227$  according to the geometry of the electron cloud, a sphere or a slab, respectively; see Table 1 for the sphere). The cause of it is that the derived electron temperature,  $kT = 239_{-60}^{+59}$  keV for a sphere and  $kT = 251_{-36}^{+86}$  keV for a slab, is too much large to account for the observed cutoff at an energy of  $\sim 100$  keV (see also Figure 5).

Then we tested the thermal-Compton model (COMPPS v3.4<sup>11</sup>) of Poutanen & Svensson (1996). The advantage of this model is that, in addition to allow for different geometries of the electron cloud, it allows for the presence of Compton reflection (Magdziarz & Zdziarski 1995) from a cold medium (like an accretion disk) with variable element abundances with respect to the solar ones. We considered spherical or slab geometries with blackbody seed photons distributed homogeneously in the plasma and the Thomson optical depth,  $\tau$ , corresponding to the radius or the half-thickness, respectively. Initially we assumed reflection from a medium with solar abundances. For consistency, we also allowed for a narrow Gaussian line ( $\sigma = 0.01$  keV) at 6.4 keV. In the spherical geometry and allowing the presence

<sup>11</sup>COMPPS is available on the internet at <ftp://ftp.astro.su.se/pub/juri/XSPEC/COMPPS>.



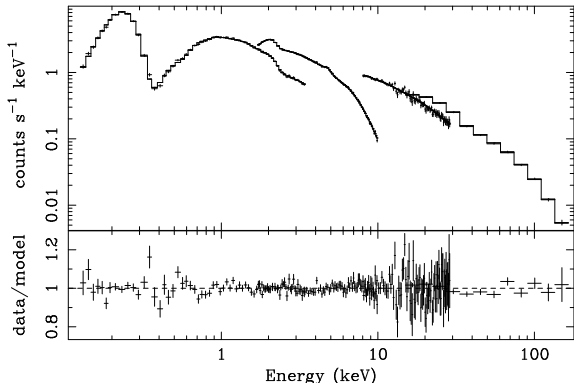


Fig. 6.— *Top panel:* The 0.1–200 keV count rate spectrum of XTE J1118+480, superposed with the best fit model consisting of an absorbed BB plus COMPPS model in the spherical geometry and a solar metal abundance (see text). *Bottom panel:* Ratio between the count spectrum and the model.

of additional blackbody photons (apart from those irradiating the plasma), we find  $\chi^2/\nu = 255/225$  at  $kT = 58_{-6}^{+12}$  keV, see Table 1. Thus the best fit provides a lower value of the electron temperature, that allows a better description of the observed high energy cutoff with respect to the COMPTT model<sup>12</sup>, see Figure 6. An F-test for 2 additional parameters provides a value of  $4.6 \times 10^{-4}$  for the probability that the  $\chi^2$  reduction from BB + COMPTT to BB + COMPPS is due to chance.

Similarly we cannot exclude the slab geometry for the same model, that provides a statistically similar fit,  $\chi^2/\nu = 263/225$ , even if the latter model seems to show in correspondence of the 150–200 keV data point a positive residual that is not observed in the case of the spherical geometry (see Figure 6).

No evidence of relative reflection was found with the above model in both geometries, with a  $2\sigma$  upper limit of  $\sim 0.16$  (see Table 1). This result, caused by the absence of an Fe K edge, contrasts other black black hole binaries in the hard state (e.g., Gierliński et al. 1997). To check the robustness of the absence of reflection, we first consider

the dependence on the inclination. We find no evidence of relative reflection even at  $i = 79^\circ$  (about the maximum allowed by the data, §2.1) with a  $2\sigma$  upper limit of 0.26. Also no evidence of a narrow Fe K line is found in the data, with a  $2\sigma$  upper limit of the line intensity of  $2.4 \times 10^{-4}$  photons  $\text{cm}^{-2} \text{s}^{-1}$  with energy from 6.4 to 6.9 keV, independently of the geometry adopted (see Table 1).

A low metal abundance,  $Z$ , of the reflecting medium is expected for halo stars, like XTE J1118+480. Spectrally, it has an effect of reducing the K edge in the reflected spectral component without changing the shape of its high-energy cutoff. We find that allowing for  $Z < Z_\odot$  only slightly improves the fit bringing  $\chi^2/\nu$  to 247/225 (246/225) in the spherical (slab) geometry. Table 1 shows the best fit parameters in both geometrical configurations. We are not capable to discriminate between these geometries. We now observe a statistically significant Compton reflection, similar to the upper limits found when  $Z/Z_\odot$  was fixed to 1. We notice that the Comptonization parameters are slightly lower than those found with Cyg X-1 in the hard state (Gierliński et al. 1997), in the assumption of a single temperature isotropic model. The fit with variable  $Z$  is shown in Figure 7, which also shows the remaining small residuals.

We have also considered a multi-component model consisting of the COMPPS model in which the spectrum of seed photons peaks below the observed range ( $kT_{\text{seed}}$  fixed at 10 eV), plus an additional BB component plus the narrow Gaussian profile (see above) at 6.4 keV. Such a low energy of seed photons is expected, e.g., when Comptonization of thermal synchrotron emission dominates (e.g. Wardziński & Zdziarski 2000), see §6. This model, in both geometries (sphere or slab), yields a good description of the data as the last model, with a  $\chi^2/\nu = 244/224$ . The best fit parameters are reported in Table 1. Notice the value of  $N_{\text{H}}$  in the slab geometry ( $= 1.73_{-0.35}^{+0.31} \times 10^{20} \text{ cm}^{-2}$ ) which is somewhat above  $N_{\text{H,G}}$ .

Leaving the metallicity free to vary, we have also tested for the effect of replacing the blackbody spectrum by a disk blackbody, in this case assuming the seed photons for Comptonization to be also those of the disk blackbody. This model yields plasma parameters very similar to the blackbody case above and a similar fit quality ( $\chi^2/\nu =$

<sup>12</sup>Note that the values of  $kT$  obtained with COMPPS are much lower from that derived from COMPTT, which is caused by inaccuracies in the shape of the high-energy cutoff in the latter model, see, e.g., Zdziarski, Johnson, & Magdziarz (1996).

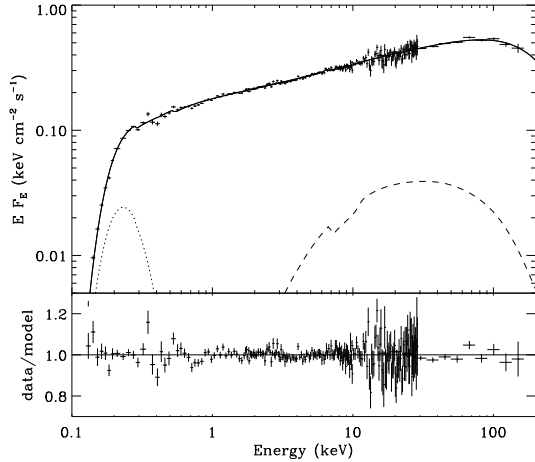


Fig. 7.— The *BeppoSAX* spectrum (crosses) fitted by (solid curve) a blackbody at 36 eV plus a thermal Comptonization in the slab geometry and a Compton reflection from a low-metallicity medium. The latter is shown separately by the dashed curve while the blackbody is shown by a dotted line. The spectrum is normalized to the level of the MECS (see text). The bottom panel shows the fit residuals.

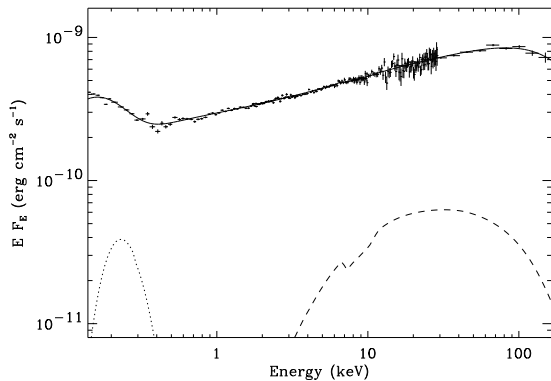


Fig. 8.— The absorption-corrected model spectrum (solid curve) corresponding to the fit shown in Fig. 7. The dashed curve shows the Compton reflection component, while the dotted curve shows the blackbody spectrum observed. The initial (i.e., before Compton scattering) spectrum of the seed photons incident on the plasma corresponds to the peak at  $\sim 0.15$  keV.

244/224 for a slab and = 245/224 for a sphere). The inner disk temperature is  $kT_{\text{in}} = 41_{-4}^{+3}$  eV at an inner radius greater than  $\sim 500$  km (scaled at  $d = 1.5$  kpc), that corresponds to  $\sim 34R_g$  ( $R_g \equiv GM_X/c^2$ ), assuming  $M_X = 10M_\odot$ .

The absorbing columns fitted in models using COMPPS are close the Galactic  $N_{\text{H}}$ , with some absorption intrinsic to the source possible as well. We note that the value of  $2.8 \times 10^{20} \text{ cm}^{-2}$  favored by Dubus et al. (2001) is inconsistent with our data, yielding, e.g.,  $\chi^2/\nu = 308/226$  in the model with Comptonization in the spherical geometry. This confirms our independent conclusions of §2.2.

From the overall best-fit models, the mean flux level of the source during the observation is  $5.7 \times 10^{-10} \text{ erg cm}^{-2} \text{ s}^{-1}$ ,  $6.9 \times 10^{-10} \text{ erg cm}^{-2} \text{ s}^{-1}$ ,  $1.9 \times 10^{-9} \text{ erg cm}^{-2} \text{ s}^{-1}$ , and  $3.4 \times 10^{-9} \text{ erg cm}^{-2} \text{ s}^{-1}$  in the 0.1–2 keV, 2–10 keV, 15–200 keV, and 0.1–200 keV bands, respectively (normalized to the MECS detector). The total (0.01– $10^3$  keV) flux corrected for absorption is somewhat model-dependent, and it equals to  $4.2 \times 10^{-9} \text{ erg cm}^{-2} \text{ s}^{-1}$  for the BB + COMPPS model in the slab configuration ( $Z/Z_{\text{sun}}$  free to vary in the fit) (see Table 1 and fig.7). The absorption-corrected flux of the observed blackbody is  $2.2 \times 10^{-10} \text{ erg cm}^{-2} \text{ s}^{-1}$  to be compared with a flux of  $3.8 \times 10^{-10} \text{ erg cm}^{-2} \text{ s}^{-1}$  due to blackbody photons incident on the hot plasma, i.e. 9% of the total flux (with an apparent amplification factor of 11).

A temporal analysis of the data with Fourier techniques shows that the fractional variation of the source flux in the 0.01–50 Hz frequency range and the 2–10 keV energy band is 42% rms, which is consistent with the findings by Revnivtsev et al. (2000). In the 0.1–2 keV range, the fractional variation is even higher (62% rms). Also, a QPO with the centroid frequency at  $\sim 0.08$  Hz is apparent in our power spectral density estimate. We do not find any statistically significant modulation at the optical period of 0.17 day. This implies that the X-ray source is axially symmetric and no absorption in the line of sight is associated with the outflow of matter from the companion star.

## 5. Spectral comparison with *RXTE* data

*RXTE* performed many short pointings of XTE J1118+480. McClintock et al. (2001b) reported spectral results on this source based on the ob-

servation of April 18.8111–18.9583 UT and, for the study of the high energy part of the spectrum ( $>100$  keV), results of the summed spectra obtained between April 13.39 UT and May 15.39 UT. No evidence of a high energy cut-off was found in the summed spectra, while the high energy data of the April 18 observation were affected by large uncertainties (see figure 4 of McClintock et al. 2001).

One of the *RXTE* pointings of XTE J1118+480 was performed simultaneously with a part of our observation. The *RXTE* observation (see, e.g., Revnivtsev et al. 2000) started 2000 April 15 7:57:52 UT, and had an exposure time of 1152 s for the PCA, and 378 s and 361 s for the 2 High Energy X-ray Timing Experiment (HEXTE) clusters, respectively. A detailed study of this and other *RXTE* observations of XTE J1118+480 will be given elsewhere. We first fitted the *RXTE* spectrum by an e-folded power law, obtaining  $\Gamma \simeq 1.8$ , i.e., a higher index than  $\Gamma \simeq 1.7$  for the *BeppoSAX* spectrum (Table 1). This difference is likely to be of instrumental origin, as a similar difference between the PCA and other X-ray instruments is commonly found in fits to the Crab as well as other sources (e.g., Gierliński et al. 1999; Done, Madejski, & Życki 2000).

Then, we fit the 3–200 keV data with Comptonization in the spherical geometry, Compton reflection at  $Z_{\odot}$ , and a narrow Fe  $K\alpha$  line. We obtain  $\Omega/2\pi = 0.05$  at the best fit, confirming the weakness of Compton reflection. However, the fitted electron temperature is somewhat larger than that of the *BeppoSAX* data,  $kT = 190_{-80}^{+50}$  keV. We find, however, that if apply a correction of  $\Delta\Gamma = 0.1$  to the model fitted to the PCA data,  $kT$  becomes equal to  $140_{-100}^{+60}$  keV, consistent with the values of  $kT$  in Table 1. The large confidence regions of  $kT$  are due to the limited statistics of the HEXTE data (the *RXTE* observation lasted only a small fraction of the *BeppoSAX* one). The fact that the summed *RXTE* spectra (covering more than a month elapsed time) are still described by a power law with no high energy cut-off below  $\sim 150$  keV (McClintock et al. 2001) could be the result of the evolution of the source spectrum. In fact our preliminary results of the later 2 observations of the source (see fig. 1) show a decreasing evidence of the high energy cut-off with time (Frontera et al. 2001b).

Summarizing, also the *RXTE* data appear to be

compatible with the *BeppoSAX* ones, especially when the difference in the calibration between the PCA and *BeppoSAX* is taken into account.

## 6. Theoretical Implications

The Eddington luminosity at an H mass fraction of 0.7 can be written as

$$L_E \simeq 1.5 \times 10^{39} (M_X/10M_{\odot}) \text{ erg s}^{-1}, \quad (8)$$

and the gravitational radius is

$$R_g \equiv GM_X/c^2 \simeq 15(M_X/10M_{\odot}) \text{ km}. \quad (9)$$

The total X-ray luminosity corrected for absorption calculated using the Comptonization model shown in Fig. 8 and assuming isotropy is

$$\begin{aligned} L_X &\simeq 1.1 \times 10^{36} (d/1.5 \text{ kpc})^2 \text{ erg s}^{-1} \\ &\simeq 8 \times 10^{-4} \left( \frac{d}{1.5 \text{ kpc}} \right)^2 \left( \frac{M_X}{10M_{\odot}} \right)^{-1} L_E. \end{aligned} \quad (10)$$

Here we used the estimates for the black hole mass and the source distance (§2.1). We note that the  $L_X$  above does not represent the bolometric luminosity of the source, whose  $EF_E$  spectrum has been observed by Hynes et al. (2000) to have a maximum in the far UV at a level similar to that of the peak at  $\sim 100$  keV. Given their results, the bolometric luminosity can be estimated as  $\sim 2L_X$ . Still,  $L_X$  represents the luminosity of the hot plasma flow.

A fundamental issue is the geometry of the source. The weakness of Compton reflection and of blackbody emission poses some constraints. There are two possible solutions we can envisage. The direct emission from the accretion disk is smeared by Compton scattering in the corona, or the hot gas subtends a small solid angle by a cold medium.

A static disk/corona geometry (e.g., Haardt & Maraschi 1991), similar to the case of Cyg X-1 in the hard state, can be reconciled with the data, as the large value of  $\tau/\cos i$  would scatter most of the reflection and blackbody emission in the power law continuum. However, because of the tight coupling of the hot and cold phases, this model cannot produce a spectrum as flat as that observed. In principle, a mildly relativistic coronal outflow can alleviate the problem (Beloborodov 1999; Malzac, Beloborodov, & Poutanen 2001).

Given that, the specific coronal model of Merloni, Di Matteo, & Fabian (2000) has some difficulties. It can produce a flat spectrum, but, as it postulates magnetic flares in a disk-corona geometry, it predicts the presence of a strong blackbody component about an order of magnitude above that observed, even with relativistic bulk motion of the flares taken into account (compare their Fig. 1 with our Fig. 8).

On the other hand, the observed spectrum is fully compatible with Compton scattering in a hot central disk. Indeed, this is the geometry of our overall best-fit model. Then, the weakness of the blackbody and Compton–reflection components is naturally accounted for by a small solid angle subtended by any cold medium as seen from the hot disk. An important issue here is the origin of the seed photons. The weakness of the blackbody corresponds to rather small size of the cold region. In either the blackbody or disk-blackbody model (see §4 and Table 1), the characteristic radius of the blackbody emitter is  $\geq \sim 30R_g$  (at  $d = 1.5$  kpc,  $M = 10M_\odot$ ) for our best fit models. Thus, the seed photons can be supplied by an outer cold disk, probably overlapping with the hot one.

Another compatible source of seed photons compatible is thermal synchrotron emission of the hot plasma itself (which naturally produces homogeneous and isotropic seed photons). Then the soft excess found in the data can represent either the peak of the self-absorbed thermal synchrotron emission (e.g. Wardziński & Zdziarski 2000) or blackbody emission not related to the dominant source of seed photons. The latter model was found in §4 to provide a good fit to the data. In fact, Wardziński & Zdziarski (2000) have predicted that the thermal synchrotron process is able to dominate the supply of seed photons at an intermediate range of Eddington factors,  $L_X/L_E \lesssim 10^{-3}$ , compatible with the case in XTE J1118+480.

By considering the synchrotron process, we can constrain the magnetic field strength in the source. The turnover energy,  $E_t$ , at which the thermal self-absorbed synchrotron emission peaks, is approximately

$$E_t \simeq 1.3 \left( \frac{kT}{10^2 \text{keV}} \right)^{0.95} \tau^{0.05} \left( \frac{B}{10^6 \text{G}} \right)^{0.91} \text{eV} \quad (11)$$

(Wardziński & Zdziarski 2000). This yields a con-

straint on the magnetic field strength of  $B \lesssim 10^8$  G, with the approximate equality corresponding to the observed soft excess at  $\sim 0.15$  keV (Fig. 8) being due to the turnover peak and no non-thermal electron tail. For lower values of  $B$ , the observed soft excess is due to blackbody emission. Then, the UV data of Hynes et al. (2000) constrain  $E_t \gtrsim 10$  eV. Wardziński & Zdziarski (2001) have found that  $E_t$  of equation (11) can increase by a factor of  $\sim 2$ –3 in the presence of a weak non-thermal tail beyond the Maxwellian electron distribution (with a corresponding high-energy photon tail observed in Cyg X-1, McConnell et al. 2000). Then, the UV constraint implies  $B \gtrsim 10^7$  G in the absence of a non-thermal tail and  $B \gtrsim 3 \times 10^6$  G with a tail. Only lower values of the above range of  $B$  correspond to equipartition in a hot accretion flow with moderately sub-virial ions [e.g., eq. (34) in Wardziński & Zdziarski 2000], which indicates that the observed soft X-ray excess is due to a separate blackbody component rather than the turnover peak at  $E_t$ . Summarizing,  $B \lesssim 10^8$  G is implied directly by the data, and  $B \gtrsim (3\text{--}10) \times 10^6$  G for the synchrotron process to be the dominant source of seed photons.

The high erratic time variability we find in the soft X-ray band (as well as in hard X-rays) points out to the origin of soft X-ray excess in the same spatial region as that occupied by the hot plasma. This is in agreement with both the seed photons being provided by the blackbody emission of clouds within the hot plasma or their origin from the synchrotron process. The latter model also agrees with a similar time variability observed in the optical band, as noted by Merloni et al. (2000).

Within the Compton scattering model in a hot central disk, our data appear compatible with the hot disk being advection-dominated, as recently proposed by Esin et al. (2001) on the basis of near-simultaneous *HST*, *EUVE*, *Chandra* and *RXTE* observations. However, if such interpretation is correct, it is not clear how to compare this result with Cygnus X-1, which has a much larger luminosity and almost the same spectral parameters (Esin et al. 1998; Frontera et al. 2001a).

McClintock et al. (2001b) reported a break at about 2 keV in the  $EF(E)$  spectrum of XTE J1118+480, which was interpreted by Esin et al. (2001) as due to the presence of a warm absorber. The data used by McClintock et al. (2001b) were

obtained combining together different instruments aboard different missions. We do not see this break (see Figure 8), that could also be due to cross-calibration problems.

## 7. Conclusions

Our main findings can be summarized as follows.

We find the Galactic column density of HI measured in radio in the direction to the source as  $N_{\text{H}} \simeq (1.28\text{--}1.44) \times 10^{20} \text{ cm}^{-2}$  (Dickey & Lockman 1990) to be consistent with spectral fitting of our *BeppoSAX* data (see Table 1). On the other hand, we find the value of  $2.8 \times 10^{20} \text{ cm}^{-2}$  favored by Dubus et al. (2001) based on their measurement of Ca absorption to be intrinsically highly uncertain (§2.2) as well inconsistent with our data (§4).

Our *BeppoSAX* spectrum of XTE J1118+480 shows a power law with  $\Gamma \simeq 1.7$  modified by a soft X-ray excess and a high energy cutoff, with both features highly significant statistically. The soft excess contains a small fraction of the total flux, and is consistent with a blackbody component, either undergoing Comptonization or not. The high energy cutoff is well fitted by Comptonization in a thermal plasma with an electron temperature of  $\sim 10^2 \text{ keV}$  and a Thomson optical depth of  $\tau \sim 1$ . In agreement with the weakness of the blackbody, Compton reflection is weak, also consistent with the weakness of an Fe  $K\alpha$  line. The low amplitudes of all the features originating in the cold matter can have several explanations. If such components come from an underlying accretion disk, the relative large  $\tau$  and inclination angle easily dim the observable reflection and blackbody features by a factor  $\exp(-\tau/\cos i) \simeq 0.1$ , consistent with our observations. However, in this case, the resulting Compton spectrum would be steeper than observed. A possibility is that any cold matter subtends a small solid angle as seen by the hot gas. In this case the seed photons for Comptonization can be provided by an outer cold disk, or by synchrotron emission internal in the hot disk, or both. If the geometry is that of a central hot disk, it is not clear if our data are consistent with the ADAF solution, or instead if they rather indicate a radiative cooled hot accretion disk.

The data are statistically consistent with the

reflector to have a low metallicity,  $Z/Z_{\odot} \sim 0.1$ , as expected due to the high latitude of the system. This could be an important finding, which should be tested by future observations of the secondary.

The values of  $kT$  and  $\tau$  we find are very similar to those typical of most luminous (e.g.,  $L_{\text{X}} \sim 0.02L_{\text{E}}$  in Cyg X-1) black-hole binaries in the hard state, whereas the X-ray luminosity in our measurement is only  $\sim 10^{-3}L_{\text{E}}$ .

We thank Juri Poutanen for valuable discussions, and Grzegorz Wardziński for reducing the *RXTE* data used in §5. The *BeppoSAX* program is supported by the Italian Space Agency (ASI). AAZ and JM have been supported in part by KBN grants 2P03D00614 and 2P03C00619p0(1,2) and a grant from the Foundation for Polish Science. FF, FH and LS acknowledge a financial support from the Ministry of University and Scientific Research of Italy (COFIN 2000).

## REFERENCES

- Anders, E., & Ebihara, M. 1982, *Geochim. Cosmochim. Acta*, 46, 2363
- Arnaud, K. A. 1996, in *ASP Conf. Series 101, Astronomical Data Analysis Software and Systems V*, ed. G. H. Jacoby & J. Barnes (San Francisco: ASP), 17
- Baraffe, I., & Chabrier, G. 1996, *ApJ*, 461, L51
- Baraffe, I., & Kolb, U. 2000, *MNRAS*, 318, 354
- Beloborodov, A. M. 1999, *ApJ*, 510, L123
- Beuermann, K., Baraffe, I., Kolb, U., & Weichhold, M. 1998, *A&A*, 339, 518
- Boella, G., et al. 1997, *A&AS*, 122, 327
- Chaty, S., et al. 2000, *IAU Circ.* 7394
- Cook, L., et al. 2000, *IAU Circ.* 7397
- Dickey, J. M., & Lockman, F. J. 1990, *ARA&A* 28, 215
- Done, C., Madejski, G. M., & Życki, P. T. 2000, *ApJ*, 536, 213
- Dubus, G., Kim, R. S. J., Menou, K., Szkody, P., & Bowen, D. V. 2001, *ApJ*, submitted (astro-ph/0009148)
- Esin, A. A., Narayan, R., Cui, W., Grove, J. E., & Zhang, S. N. 1998, *ApJ*, 505, 854
- Esin, A. A., McClintock, J. E., Drake, J. J., Garcia M. R., Haswell, C. A., Hynes, R. I., & Munro, M. P. 2001, *ApJ*, in press (astro-ph/0103044)

- Faison, M. D., Goss, W. M., Diamond, P. J., & Taylor, G. B. 1998, *AJ*, 116, 2916
- Frank, J., King, A., & Raine, D. 1992, *Accretion Power in Astrophysics* (Cambridge: Cambridge University Press)
- Frontera, F., et al. 1997, *A&AS*, 122, 357
- Frontera, F., et al. 2001a, *ApJ*, 546, 1027
- Frontera, F., et al. 2001b, *Proc. 4th INTEGRAL Workshop*, in press.
- Garcia, M., et al. 2000, *IAU Circ.* 7392
- Garnavich, P. M. 2000, *IAU Circ.* 7542
- Gierliński, M., Zdziarski, A. A., Done, C., Johnson, W. N., Ebisawa, K., Ueda, Y., Haardt, F., & Philips, B. F. 1997, *MNRAS*, 288, 958
- Gierliński, M., Zdziarski, A. A., Poutanen, J., Coppi, P., Ebisawa, K., & Johnson W. N. 1999, *MNRAS*, 309, 496
- Haardt, F., & Maraschi, L. 1991, *ApJ*, 380, L51
- Haswell, C. A., Hynes, R. I., & King, A. R. 2000a, *IAU Circ.* 7407
- Haswell, C. A., et al. 2000b, *IAU Circ.* 7427
- Hynes, R. I., Mauche C. W., Haswell, C. A., Shrader, C. R., Cui, W., & Chaty, S. 2000, *ApJ*, 539, L37
- Kuulkers, E. 2001, *Astr. Nachr.* 322, 9 (*astro-ph/0102066*)
- Magdziarz, P., & Zdziarski, A. A. 1995, *MNRAS*, 273, 837
- Malzac, J., Beloborodov, A. M., & Poutanen, J. 2001, *MNRAS*, in press
- Manzo, G., et al. 1997, *A&AS*, 122, 341
- McClintock, J., Garcia, M., Zhao, P., Caldwell, N., & Falco, E. 2000, *IAU Circ.* 7542
- McClintock, J. E., Garcia, M. R., Caldwell, N., Falco, E. E., Garnavich, P. M., & Zhao, P. 2001a, *ApJ*, submitted (*astro-ph/0101421*) [M01a]
- McClintock, J. E., et al. 2001b, *ApJ*, submitted (*astro-ph/0103051*)
- McConnell, M. L., et al. 2000, *ApJ*, 543, 928
- Merloni, A., Di Matteo, T., & Fabian, A. C. 2000, *MNRAS*, 318, L15
- Morrison, R., & McCammon, D. 1983, *ApJ*, 270, 119
- Narayan, R., & Yi, I. 1995, *ApJ*, 452, 710
- Parmar, A. N., et al. 1997, *A&AS*, 122, 309
- Pooley, G. G., & Waldram, E. M. 2000, *IAU Circ.* 7390
- Poutanen, J., & Svensson, R. 1996, *ApJ*, 470, 249
- Pringle J. E., 1976, *MNRAS*, 177, 65
- Remillard, R. A., et al. 2000, *IAU Circ.* 7389
- Revnivtsev, M., Sunyaev, R., & Borozdin, K. 2000, *A&A*, 361, L37
- Schlegel, D.J., Finkbeiner, D.P. & Davis, M. 1998, *ApJ*, 500, 525
- Sembach, K. R., & Danks, A. C. 1994, *A&A*, 289, 539
- Shapiro, S. L., Lightman, A. P., & Eardley, D. M. 1976, *ApJ*, 204, 187
- Smak, J. 1981, *Acta Astr.*, 31, 395
- Svensson, R., & Zdziarski, A. A. 1994, *ApJ*, 436, 599
- Tanaka, Y., & Shibazaki, N. 1996, *ARA&A*, 34, 607
- Titarchuk, L. G. 1994, *ApJ*, 434, 570
- Uemura, M., et al. 2000, *PASJ*, 52, L15
- van Paradijs, J., & McClintock, J. E. 1995, in *X-ray Binaries*, ed. W. H. G. Lewin, J. van Paradijs & E. P. J. van den Heuvel (Cambridge: Cambridge University Press), 58
- Wagner, R. M., Foltz, C. B., Starrfield, S. G., & Hewett, P. 2000, *IAU Circ.* 7542
- Wardziński, G., & Zdziarski, A. A. 2000, *MNRAS*, 314, 183
- Wardziński, G., & Zdziarski, A. A. 2001, *MNRAS*, in press
- Wilson, R. E. 1990, *ApJ*, 356, 615
- Wilson, C. A., & McCollough, M. L. 2000, *IAU Circ.* 7390
- Wood, K. et al. 2000, *ApJ*, 544, L45
- Wren, J., & McKay, T. 2000, *IAU Circ.* 7394
- Zdziarski, A. A. 2000, in *IAU Symp. 195, Highly Energetic Physical Processes and Mechanisms for Emission from Astrophysical Plasmas*, ed. P. C. H. Martens, S. Tsuruta & M. A. Weber (San Francisco: ASP), 153 (*astro-ph/0001078*)
- Zdziarski, A. A., Johnson, W. N., & Magdziarz, P. 1996, *MNRAS*, 283, 193

---

This 2-column preprint was prepared with the AAS L<sup>A</sup>T<sub>E</sub>X macros v5.0.